Dyes and Pigments 167 (2019) 1–9

Contents lists available at ScienceDirect

Dyes and Pigments

journal homepage: www.elsevier.com/locate/dyepig

Mechanofluorochromism based on BOPIM complexes: The effect of substituents and regulation of the direction of the emission color changes

Yong Zhan[a,*], Xin Wang[b], Yunhan Wang[b], Yongnan Xu[b]

[a] Department of Pharmacy, College of Life Sciences, China Jiliang University, Hangzhou, 310018, PR China

[b] Key Laboratory of Structure-Based Drug Design and Discovery, Ministry of Education, Shenyang Pharmaceutical University, Shenyang, 110016, PR China

ABSTRACT

Novel boron 2-(2′-pyridyl)imidazole (BOPIM) complexes **T1**, **T2** and **T3** with different substituents (including bromo, *tert*-butyl and methoxyl) on the benzene ring of BOPIM dyes have been designed and synthesized, and their optical properties in both solution and the solid state were investigated and compared. The three compounds exhibited typical intramolecular charge transfer (ICT) characteristics. Solvent-dependent UV-vis absorption, fluorescence emission spectra and quantum chemical calculation indicated a molecular push-pull electronic structure. Their ICT degrees increased with the sequence of **T1** < **T2** < **T3**. The analysis of the X-ray crystal structure revealed the twisted molecular conformation of BOPIM dyes. Furthermore, they showed remarkable reversible mechanofluorochromic (MFC) features under mechanical force. It was found that the MFC activities could be tuned easily by changing the substituents on the BOPIM dyes. **T1** exhibited emission color change from bright green to yellowish green with a spectral red-shift of only 22 nm under mechanical stimuli, whereas **T2** and **T3** gave the large spectral red-shifts of 36 and 30 nm. Electronic and steric effects of the substitutes were proved playing significant roles in regulating the ICT effect and intermolecular interactions. More importantly, the remarkable effect of substituents on the MFC behaviors of BOPIM dyes will provide an effective way to obtain novel high-contrast MFC dyes.

1. Introduction

In recent years, the exploitation of solid-state fluorescent organic materials has attracted a great deal of attention due to their potential application in photoelectronic devices and sensors [1]. Among these materials, mechanofluorochromic (MFC) materials exhibiting variable colors in response to external forces are attracting intensive interest due to their potential applications in sensors, memory chips and security systems [2]. Up to now, various kinds of π-conjugated organic molecule such as tetraphenylethene [3], triphenylacrylonitrile [4], cyanoethylene [5], 9,10-divinylanthracene [6] and difluoroboron *β*-diketone (BF_2dbk) boron complexes [7] have been found to show obvious mechanochromic luminescence change under mechanical force stimuli. The molecular structure, conformation, packing modes and intermolecular interactions play an important role in modulating fluorescence under mechanical forces [8]. A short synthetic route and simple molecular structure are preferred. However, there are extremely rare of clear design strategy of already reported MFC materials [9]. Investigations on the groups of structural analogues are usually an effective way to understand the MFC mechanisms and explain the corresponding structural feature [10].

Recently, organoboron fluorescent dyes have attracted considerable attention because of their high fluorescence yield, large absorption coefficient and excellent photochemical stability [11]. However, typical boron-difluoride molecule (BODIPY) feature high degree of planarity, resulting in fluorescent quenching in the aggregated state [12]. Generally, the strong emission in the solid state is the prerequisite for excellent MFC materials. Thus, a series of boron 2-(2′-pyridyl)-imidazole (BOPIM) complexes with strong fluorescent emission in the solid state might be candidates for MFC materials [13]. These molecules not only have high fluorescence quantum yield, large Stokes shift, and good thermal stability, but also can interact with adjacent molecules through multiple intermolecular non-covalent bondings to significantly alleviate π-π stacking-induced fluorescence quenching [14]. To date, BOPIM dyes are rarely explored as MFC materials. In addition, structural tailoring of BOPIM dyes for fine-tuning of their photophysical properties has offered great chances toward organic fluorescent materials. With these in mind, herein, we reported the synthesis, photophysical properties and MFC behaviors of three BOPIM based fluorescent dyes (**T1**, **T2** and **T3**, Fig. 1), in which different substituents (including bromo, *tert*-butyl and methoxyl) are selected to attach to the benzene ring of BOPIM dyes. These compounds exhibited high fluorescence quantum yield in both solution and the solid state. The optical properties of BOPIM dyes were studied and compared. The emission color could be tuned via the introduction of different substituents on the BOPIM dyes. The single crystal structure of **T1** reflected the non-planar orientation between BOPIM core and benzene rings, which leaded to close π-π stacking. It is interesting that three dyes revealed reversible

* Corresponding author.
E-mail address: zhanyong@cjlu.edu.cn (Y. Zhan).

https://doi.org/10.1016/j.dyepig.2019.04.001
Received 11 January 2019; Received in revised form 1 March 2019; Accepted 1 April 2019
Available online 08 April 2019

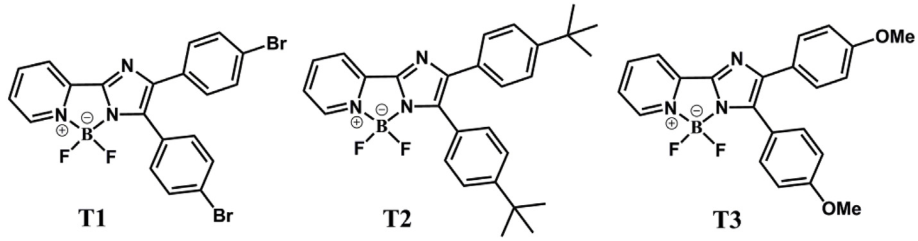

Fig. 1. Molecular structures of BOPIM dyes **T1**-**T3**.

mechanofluorochromism through grinding and solvent fuming treatment. The MFC activities of three compounds are increased in a sequence of **T1** < **T3** < **T2**. For **T1**, it showed minimum spectral redshift upon external force due to its least ICT degree in the excited state in the three luminogens. In the case of **T2** and **T3**, although **T2** exhibited the less ICT degree than **T3**, **T2** exhibited the maximum MFC behaviors. We proposed that the introduction of *tert*-butyl owing to the steric hindrance effect would lead to more loose π-π stacking in aggregated state, which was favorable for yielding efficient MFC [15]. The above results demonstrated that the MFC behaviors of BOPIM dyes were influenced by electronic and steric effects of the substitutes. Rational introduction of substituents allowed convenient modulation of photophysical properties and MFC behaviors of BOPIM dyes.

2. Experimental section

2.1. Materials and measurements

^{1}H and ^{13}C NMR spectra were measured on a Bruker AMX-400 NMR spectrometer at 600 MHz and 150 MHz in DMSO as the solvent at room temperature. FT-IR spectra were measured with a Nicolet-360 FT-IR spectrometer by the incorporation of samples in KBr disks. High resolution mass spectrometry analysis was carried out on an Agilent 6500 Q-TOF mass spectrometer (Version Q-TOF B.05.01). The UV-vis absorption spectra were determined on a Beijing purkinje TU-1810 Spectrophotometer. Fluorescence emission spectra were obtained on a Shimadzu RF-5301 PC Spectrofluorophotometer. The fluorescence quantum yields in solvents were estimated by comparing to a standard (9,10-diphenyl anthracene in benzene, $\Phi_F = 0.85$). The absolute fluorescent quantum yields were estimated on an Edinburgh FLS920 steady state spectrometer using an integrating sphere. Powder X-ray diffraction (XRD) measurements were carried out with a Bruker Advances D8 X-ray diffractometer. DSC measurements were carried out using a Mettler Toledo 3 thermos system at a heating rate of 10 °C/min. The frontier orbital plots of the HOMO and LUMO of **T1**, **T2**, and **T3** were obtained by density functional theory (DFT) calculations at the B3LYP/6-31G level with the Gaussian 09W program package. Single crystal of **T1** was obtained by slowing solvent evaporation in mixture of CH_2Cl_2 and petroleum ether, and selected for X-ray diffraction analysis in a Rigaku RAXIS-RAPID diffractometer using graphite-monochromated Mo-K_α radiation (λ = 0.71073 Å). The crystal was kept at room temperature during data collection. The structures were solved by the direct methods and refined on F2 by full-matrix least-square using the SHELXTL-97 program. The C, N, O and H atoms were easily placed from subsequent Fourier-difference maps and refined anisotropically. CCDC number for **T1**: 1858002. DCM was distilled over calcium hydride under nitrogen immediately prior to use. The other chemicals were used as received without further purification. The ground powders were obtained by grinding the as-prepared powders with a pestle in the mortar. The fumed samples were prepared by fuming the ground powder with DCM for 1 min.

2.2. Synthesis process

2.2.1. *2-(4,5-Bis(4-bromophenyl)-1H-imidazol-2-yl)pyridine (**L1**)*

2-Cyanopyridine (0.53 g, 5 mmol), 4-bromobenzaldehyde (1.85 g, 10 mmol) and NH_4OAc (3.85 g, 50 mmol) were dissolved in 6 mL of acetic acid and the mixture was heated at 150 °C overnight to reflux in a round-bottom flask. After cooling to room temperature, the mixture was poured into saturated solution of $NaHCO_3$ and acidified with 0.1 M hydrochloric acid. A pale yellow solid was collected by filtration and dried under vacuum. The crude product was purified by column chromatography (silica gel) using petroleum ether/ethyl acetate (v/v = 5:1) to give **L1** as a white solid (1.20 g) in a yield of 53%. ^{1}H NMR (600 MHz, TMS, DMSO-d_6) δ = 13.31 (s, 1H), 8.65 (d, J = 4.2 Hz, 1H), 8.14 (d, J = 7.8 Hz, 1H), 7.94–7.91 (m, 1H), 7.61 (d, J = 8.0 Hz, 2H), 7.53 (d, J = 8.4 Hz, 2H), 7.48–7.44 (m, 4H), 7.43–7.41 (m, 1H) (Fig. S5, ESI); HRMS (ESI): m/z = 455.1453, found: 455.9536 $[M+H]^+$ (Fig. S6, ESI).

2.2.2. *2,3-Bis(4-bromophenyl)-5,5-difluoro-5H-5l4,6l4-imidazo[1′,2′:3,4][1–3]di-azaborolo [1,5-a]pyridine (**T1**)*

To a solution of compound **L1** (1.0 g, 2.2 mmol) in dry CH_2Cl_2 (30 mL), then Et_3N (4.4 mL, 31.7 mmol) was added, and the mixture was heated under N_2 atmosphere to reflux. After that, $BF_3{\cdot}Et_2O$ (4.4 mL, 34.9 mmol) was added dropwise. The mixture was refluxed with stirring for 8 h under an atmosphere of nitrogen. After cooling to room temperature, the reaction was quenched by adding water (100 mL), and the mixture was extracted with CH_2Cl_2 (3 × 50 mL). The organic phase was dried over anhydrous $MgSO_4$. After removal of solvent, the residue was purified by column chromatography on silica gel using petroleum ether/ethyl acetate (v/v = 3:1), then recrystallized from CH_2Cl_2 and petroleum ether to afford **T1** as a green solid (0.30 g) in a yield of 27%. Mp: 228 °C (obtained from DSC); ^{1}H NMR (600 MHz, TMS, DMSO-d_6) δ = 8.92 (d, J = 5.4 Hz, 1H), 8.53 (td, J = 7.8 Hz, 1.2 Hz, 1H), 8.24 (d, J = 7.8 Hz, 1H), 7.85–7.83 (m, 1H), 7.70–7.67 (m, 2H), 7.57–7.55 (m, 2H), 7.46–7.44 (m, 4H) (Fig. S7, ESI); ^{13}C NMR (150 MHz, DMSO-d_6) δ (ppm) = 149.49, 147.20, 146.37, 145.93, 143.97, 143.39, 143.14, 137.94, 133.78, 132.42, 131.89, 130.68, 130.50, 130.02, 129.89, 125.67, 124.26, 122.25, 121.29, 120.94, 120.72, 118.60 (Fig. S8, ESI); IR (KBr, cm^{-1}): 3439, 2923, 1634, 1548, 1477, 1400, 1164, 1127, 1011, 833, 715, 591; HRMS (ESI): m/z = 502.9452, found: 503.9516 $[M+H]^+$ (Fig. S9, ESI).

2.2.3. *2-(4,5-Bis(4-tert-butylphenyl)-1H-imidazol-2-yl)pyridine (**L2**)*

By following the synthetic procedure for **L1**, **L2** was synthesized by using 2-cyanopyridine (0.53 g, 5 mmol), 4-*tert*-butylbenzaldehyde (1.62 g, 10 mmol) and NH_4OAc (3.85 g, 50 mmol) as the reagents. The crude product was purified by column chromatography (silica gel) using petroleum ether/ethyl acetate (v/v = 6:1) to give **L2** as a white solid (1.10 g) in a yield of 54%. ^{1}H NMR (600 MHz, TMS, DMSO-d_6) δ = 12.96 (s, 1H), 8.63–8.62 (m, 1H), 8.11 (d, J = 7.8 Hz, 1H), 7.91 (td, J = 7.8 Hz, 1.8 Hz, 1H), 7.51 (s, 1H), 7.49–7.47 (m, 2H), 7.47 (s, 1H), 7.43–7.41 (m, 2H), 7.39–7.37 (m, 1H), 7.35 (s, 1H), 7.33 (s, 1H), 1.32 (s, 9H), 1.29 (s, 9H) (Fig. S10, ESI); HRMS (ESI): m/z = 409.2518, found: 410.2586 $[M+H]^+$ (Fig. S11, ESI).

2.2.4. 2,3-Bis(4-(tert-butyl)phenyl)-5,5-difluoro-5H-5l4,6l4-imidazo [1′,2′:3,4] [1–3]diazaborolo [1,5-a]pyridine (T2)

This compound was synthesized following the same procedure described for the synthesis of compound **T1** from **L2** (1.0 g, 2.4 mmol), Et_3N (4.9 mL, 35.2 mmol), and $BF_3{\cdot}Et_2O$ (4.9 mL, 38.6 mmol). The crude product was purified by column chromatography on silica gel using petroleum ether/ethyl acetate (v/v = 3:1), then recrystallized from CH_2Cl_2 and petroleum ether to afford **T2** as a yellow-green solid (0.37 g) in a yield of 33%. Mp: 170 °C (obtained from DSC); ^{1}H NMR (600 MHz, TMS, DMSO-d_6) δ = 8.86 (d, J = 6.0 Hz, 1H), 8.50 (td, J = 7.8 Hz, 1.2 Hz, 1H), 8.18 (d, J = 8.4 Hz, 1H), 7.79 (t, J = 6.6 Hz, 1H), 7.49–7.46 (m, 6H), 7.36 (s, 1H), 7.35 (s, 1H), 1.32 (s, 9H), 1.29 (s, 9H) (Fig. S12, ESI); ^{13}C NMR (150 MHz, DMSO-d_6) δ (ppm) = 151.06, 149.93, 146.97, 145.64, 144.27, 144.14, 142.88, 132.83, 132.22, 128.31, 127.49, 125.93, 125.42, 125.12, 118.21, 34.85, 34.69, 31.50, 31.45 (Fig. S13, ESI); IR (KBr, cm^{-1}): 3439, 2962, 1632, 1477, 1402, 1267, 1132, 1002, 837, 707, 562; HRMS (ESI): m/z = 457.2501, found: 458.2587 $[M+H]^+$ (Fig. S14, ESI).

2.2.5. 2-(4,5-Bis(4-methoxyphenyl)-1H-imidazol-2-yl)pyridine (L3)

By following the synthetic procedure for **L1**, **L3** was synthesized by using 2-cyanopyridine (0.53 g, 5 mmol), 4-methoxybenzaldehyde (1.39 g, 10 mmol) and NH_4OAc (3.85 g, 50 mmol) as the reagents. The crude product was purified by column chromatography (silica gel) using petroleum ether/ethyl acetate (v/v = 6:1) to give **L3** as a white solid (1.20 g) in a yield of 67%. ^{1}H NMR (600 MHz, TMS, DMSO-d_6) δ = 12.95 (s, 1H), 8.63–8.62 (m, 1H), 8.11 (d, J = 7.8 Hz, 1H), 7.90 (t, J = 7.8 Hz, 1H), 7.43 (d, J = 7.2 Hz, 4H), 7.37 (s, 1H), 6.93 (s, 4H), 3.77 (s, 6H) (Fig. S15, ESI); HRMS (ESI): m/z = 357.1477, found: 358.1549 $[M+H]^+$ (Fig. S16, ESI).

2.2.6. 2,3-Bis(4-methoxyphenyl)-5,5-difluoro–5H-5l4,6l4-imidazo [1′,2′:3,4] [1–3]diazaborolo [1,5-a]pyridine (T3)

This compound was synthesized following the same procedure described for the synthesis of compound **T1** from **L3** (1.0 g, 2.8 mmol), Et_3N (5.6 mL, 40.3 mmol), and $BF_3{\cdot}Et_2O$ (5.6 mL, 39.6 mmol). The crude product was purified by column chromatography on silica gel using petroleum ether/ethyl acetate (v/v = 3:1), then recrystallized from CH_2Cl_2 and petroleum ether to afford **T3** as a yellow solid (0.38 g) in a yield of 34%. Mp: 205 °C (obtained from DSC); ^{1}H NMR (600 MHz, TMS, DMSO-d_6) δ = 8.85 (d, J = 5.4 Hz, 1H), 8.48 (t, J = 7.8 Hz, 1H), 8.16 (d, J = 7.8 Hz, 1H), 7.77 (t, J = 6.6 Hz, 1H), 7.43–7.41 (m, 4H), 7.00 (d, J = 8.4 Hz, 2H), 6.91 (d, J = 8.4 Hz, 2H), 3.80 (s, 3H), 3.76 (s, 3H) (Fig. S17, ESI); ^{13}C NMR (150 MHz, DMSO-d_6) δ (ppm) = 159.50, 158.79, 149.71, 146.92, 145.23, 144.34, 143.79, 142.86, 137.97, 132.30, 130.01, 129.94, 129.92, 129.08, 127.43, 124.92, 123.40, 118.10, 114.65, 114.37, 114.15, 55.55, 55.44 (Fig. S18, ESI); IR (KBr, cm^{-1}): 3436, 2926, 1633, 1520, 1476, 1406, 1248, 1179, 1031, 1008, 834, 787, 704, 612, 545; HRMS (ESI): m/z = 405.1460, found: 406.1550 $[M+H]^+$ (Fig. S19, ESI).

3. Results and discussion

3.1. Synthesis of T1, T2 and T3

The pivotal roles of boron (III) chelation are to render the π system planar, thereby enhancing conjugation and charge transfer along the main molecular axis. The synthetic routes of BOPIM dyes are shown in Scheme 1. Firstly, starting from the corresponding aromatic aldehydes **1–3** and 2-cyanopyridine, modification of BOPIMs relied on the formation of their 2-(1*H*-imidazol-2-yl)pyridine ligands **L1-L3** through multi-component one-pot reaction with the yields of 53%–67%. Then, the produced **L1-L3** were then directly reacted with boron difluoride diethyl ether to give **T1**, **T2** and **T3** with the yields of 27%–34% [16]. All the intermediates and target molecules were purified by column chromatography on silica gel, and the target molecules **T1**, **T2** and **T3** were characterized by ^{1}H and ^{13}C NMR, FT-IR and high resolution mass spectroscopy analyses. **T1**, **T2** and **T3** are soluble in common organic solvents, such as CH_2Cl_2, THF, toluene and DMF, but show poor solubility in alcohols and aliphatic hydrocarbon solvents.

3.2. Crystal structure of T1

In order to understanding the MFC behaviors of three compounds, we intended to obtain their single crystals, but only single crystal of **T1** was prepared by slow evaporation from the mixture of ethyl acetate and petroleum ether. The collected crystal was good enough for single crystal X-ray diffraction analysis, and the data are summarized in Table S1(ESI). Crystal information revealed that **T1** crystal belonged to a triclinic space group P-1. The single crystal structure and crystal packing diagram of **T1** are shown in Fig. 2. It was clear that the fluorine-boron(III) chelation moiety was almost a plane, however, 4- and 5-substituted benzene rings adopted a non-planar orientation with dihedral angle (30.9° for 4-position and 55.23° for 5-position substituted benzene ring) between BOPIM core and side benzene ring (Fig. S1, ESI). Therefore, **T1** adopted a non-planar conformation. As shown in Fig. 2b, the BOPIM core was arranged in an anti-parallel arrangement, with partial overlap between neighboring BOPIM core, indicating it form dimer by π-π stacking interactions [17]. The crystal packing mode showed that the unit cell of **T1** contained four molecules with the presence of weak intermolecular interactions, such as B-F…H-C (d = 3.15 Å), B-F…C (distance in the range of 2.34–2.66 Å), Br…Br (d = 3.61 Å), Br…H-C (d = 3.00 Å), C…C (d = 3.34 Å), C…H-C (d = 2.80 Å) and C-H…H-C (d = 2.28 Å) (Fig. S2, ESI). The single crystal data revealed the twisted geometry and existence of weak intermolecular interactions, resulting loose packing in the crystal state, which is a key factor influencing its MFC behavior [18].

3.3. UV-vis absorption and fluorescence emission spectra in solutions

To investigate the substituent effect on the optical properties, the normalized absorption and fluorescence emission spectra of **T1**, **T2** and **T3** in different solvents (1.0×10^{-5} M) are shown in Figs. 3 and 4 and Fig. S3 (ESI), and the corresponding photophysical data are summarized in Table S2 (ESI). As shown in Fig. 3a, it was found that the three compounds showed two major absorption bands. For example, the absorption peaks of **T1** were located at 306 nm and 398 nm in THF. The formed band might be attributed to the π-π* electronic transition, whereas the latter one could be derived from intramolecular charge-transfer (ICT) transition. In order to confirm the occurrence of CT transition, the solvent-dependent fluorescence emission spectra of BOPIM dyes are shown in the Fig. 4c and d and Fig. S3b (ESI). It was clear that the maximum emission peaks of the three compounds red-shifted with increasing polarity of the solvents. For instance, in hexane, **T1** showed a strong emission peak at 505 nm, but with the increasing solvent polarity, its fluorescence band red-shifted to 532 nm in DMF accompanied by emission bands broaden. Meanwhile, the Stokes shifts of **T1** increased from 3783 cm^{-1} in hexane to 6778 cm^{-1} in DMF (Table S2, ESI). Besides, **T1** was highly emissive in hexane with a fluorescence quantum yield (Φ_F) of 0.72 using 9,10-diphenylanthracene (Φ_F = 0.85 in benzene, λ_{ex} = 390 nm) as the standard (Table S2, ESI), but Φ_F was only 0.21 in DMF. Combined with the broadening and red-shift of the emission band, accompanied by an obvious decreasing of Φ_F and the increasing Stokes shifts in polar solvents, we deemed that ICT transition of **T1** from electron-donating groups to electron-accepting BOPIM skeleton taking place in polar solvents and the longer wavelength emissions might be assigned to ICT emissions [19]. The ICT transition peak of **T2** and **T3** red-shifted to 414 nm and 424 nm, respectively, which might be due to the increased electron-donating ability and thereby reduced the energy gaps between the excited and ground states [20]. Indeed, compared with compounds **T1** and **T2**, **T3** with the strong electron-donating methoxyl group showed the most

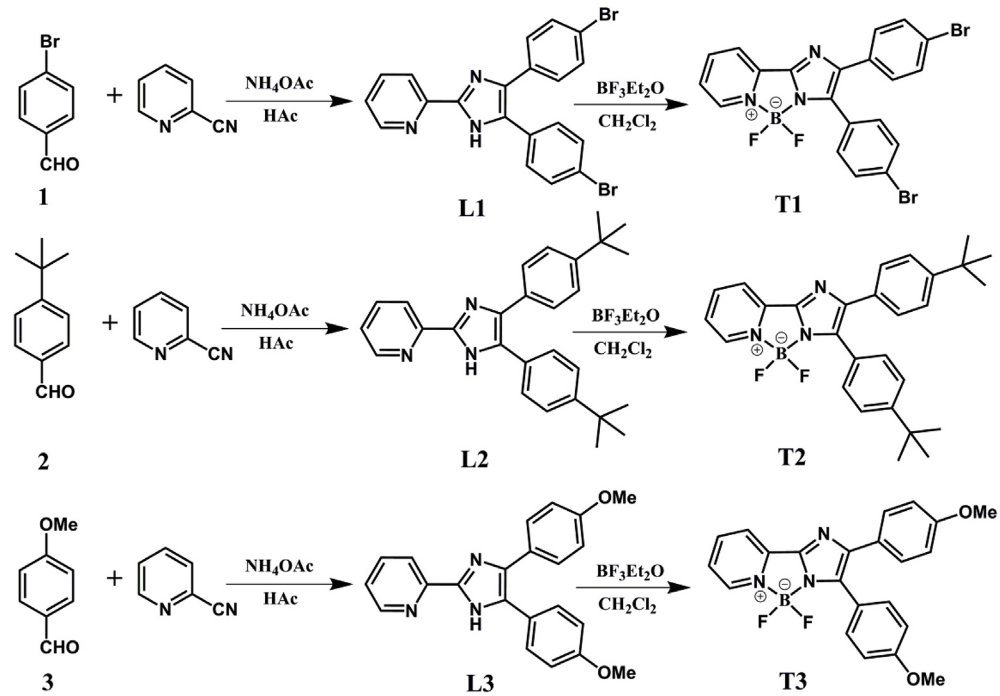

Scheme 1. Synthetic routes of **T1**, **T2** and **T3**.

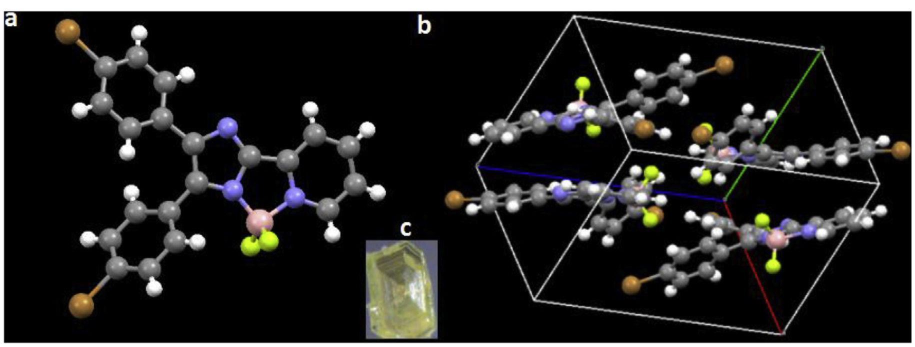

Fig. 2. (a) Single crystal structure of **T1**; (b) crystal packing diagram of **T1** with multiple intermolecular interactions. For clarity, the hydrogen atoms are not shown; (c) single crystal under natural light.

obvious variation of absorption maximum ($\Delta\lambda_{abs}$ = 42 nm) upon increasing the solvent polarity from hexane to DMF. In addition, solvatochromic effect was obtained for BOPIM dyes, that was, the lowest-energy absorption-bands were marked blue-shift with increasing solvent polarity, corresponding to classic ICT characteristics (Fig. 4a and b and Fig. S3a, ESI). Owing to their ICT feature, the PL spectra of BOPIM dyes are dependent on solvent polarity as well. As shown in Fig. 3b, it was found that the maximum emission of **T1**, **T2** and **T3** in THF located at 523 nm, 543 nm and 562 nm, respectively. The obvious bathochromic shift of **T3** should be ascribed to the increasing electron-

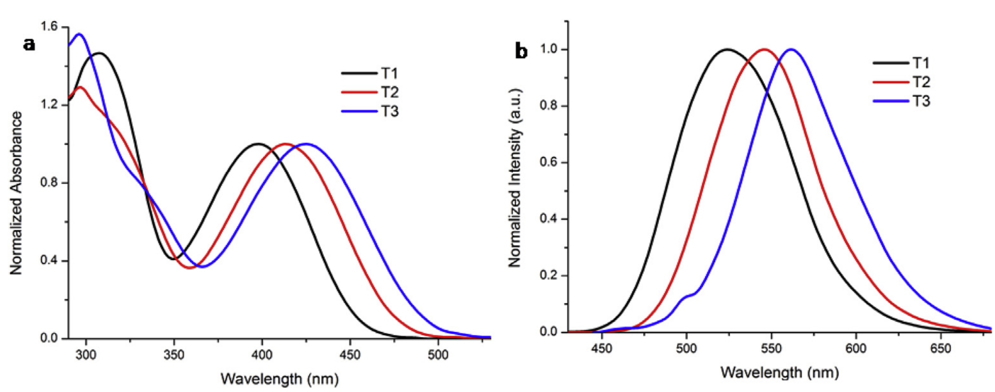

Fig. 3. (a) Normalized UV-vis absorption of **T1**, **T2** and **T3** in THF; (b) fluorescence spectra of **T1**, **T2** and **T3** (1.0×10^{-5} M, excited at 410 nm for **T1**, 420 nm for **T2** and 435 nm for **T3**) in THF.

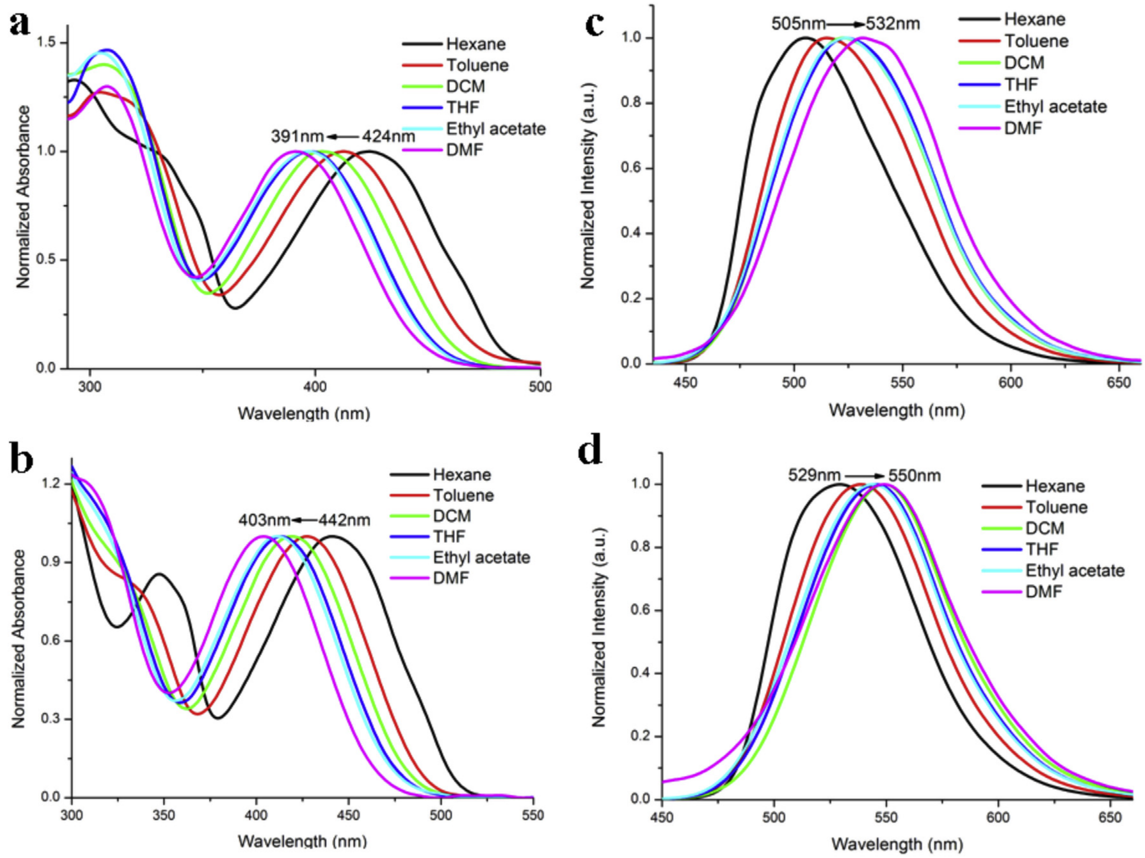

Fig. 4. Normalized UV-vis absorption spectra of **T1** (a), **T2** (b), and fluorescence emission spectra of **T1** (c, $\lambda_{ex} = 410$ nm), **T2** (d, $\lambda_{ex} = 420$ nm) in different solvents (1.0×10^{-5} M).

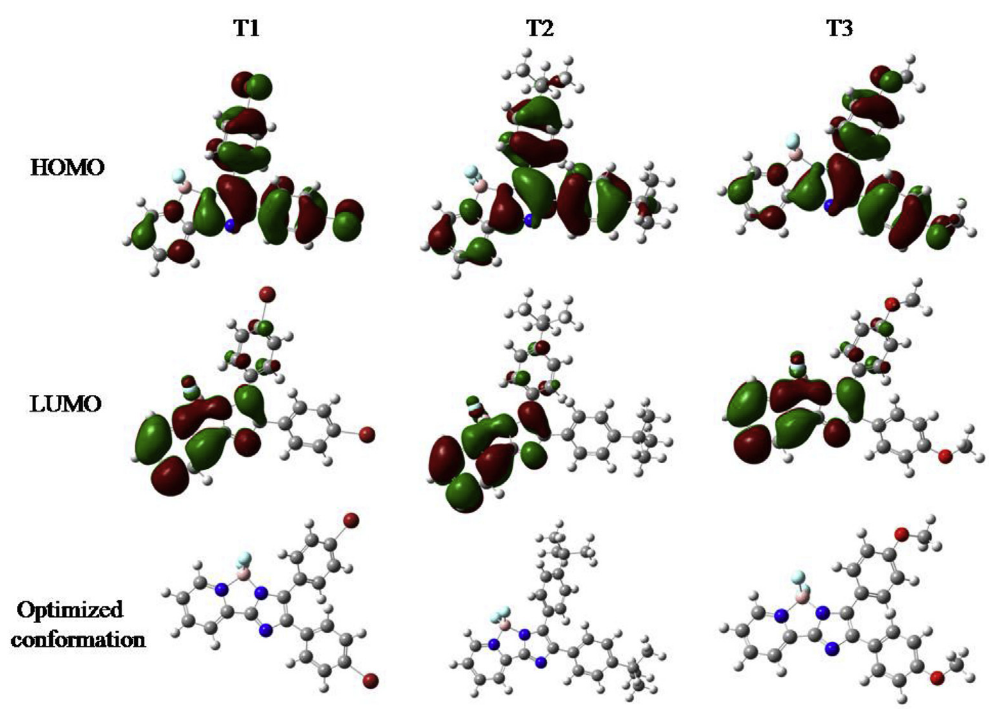

Fig. 5. Electron density distributions in the HOMO and LUMO states and optimized conformation of **T1**, **T2** and **T3** calculated by DFT in Gaussian 09W at the B3LYP/6-31G(d) level.

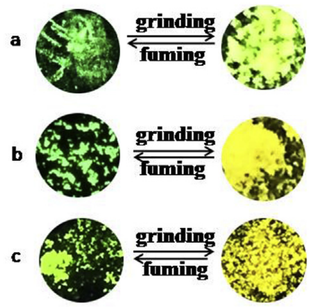

Fig. 6. Photographs of **T1** (a), **T2** (b), and **T3** (c) color changes under the treatment of grinding and fuming stimuli. (For interpretation of the references to color in this figure legend, the reader is referred to the Web version of this article.)

donating ability, which strengthens D-A effect. In addition, concerning the structure features, it is not surprised that **T1**, **T2** and **T3** showed solid state fluorescent emission with high quantum efficiency of 59.2%, 55.1%, and 46.5%, respectively.

3.4. Theoretical calculation

Density functional theory (DFT) calculations were performed on the three compounds with the Gaussian 09W package to better clarify the influence of the geometric and electronic structures of BOPIM dyes on their photophysical properties. The geometrical structures are optimized at the B3LYP/6-31G(d) level. The frontier orbital plots of the HOMO and LUMO are shown in Fig. 5, and the corresponding data are listed in Table S3 (ESI). It was found that the HOMO was mainly distributed on the 5-substituted benzene moieties, whereas the LUMO was mostly located at the boron-fluorine chromophore unit. This result demonstrated that the ICT occurred for the excited state. Compared with **T1**, the HOMO of **T2** and **T3** with the electron-donating groups showed upshift more seriously than their LUMO, respectively. Thus, the energy gaps of compound **T2** and **T3** were smaller than that of compound **T1**, which well explained that the absorption and emission bands of compounds **T2** and **T3** were longer than those of compound **T1** (Table S3, ESI). Moreover, **T3** possessed larger ICT degree in the excited state than that of **T2**. The above inference was consistent with the observed optical properties. In addition, the three compounds adopted a twisted conformation in their optimized lowest energy state, which disfavored close molecular packing and π-π interactions in the solid state [21].

3.5. Mechanofluorochromic behaviors

As discussed above, **T1**, **T2** and **T3** adopted a twisted spatial conformation in their optimized structures, thus, assembly of the molecules into closely packed structures was difficult. The crystals were easily destroyed by external force because of weak intermolecular interactions [22]. Herein, three compounds were greatly anticipated to be MFC-active materials. To investigate whether the three compounds **T1**, **T2** and **T3** exhibit mechanochromic luminescence, their emission color change in the solid state were investigated. The naked-eye-visible changes in fluorescence color were recorded and the images are shown in Fig. 6. The pristine **T1**, **T2** and **T3** solids could emit bright green, bright green and yellowish-green light under UV irradiation, their emitting colors changed into bright yellowish-green, bright yellow and yellow light, respectively, after grinding by using a spatula or a pestle, suggesting the significant MFC behaviors of the three molecules. The

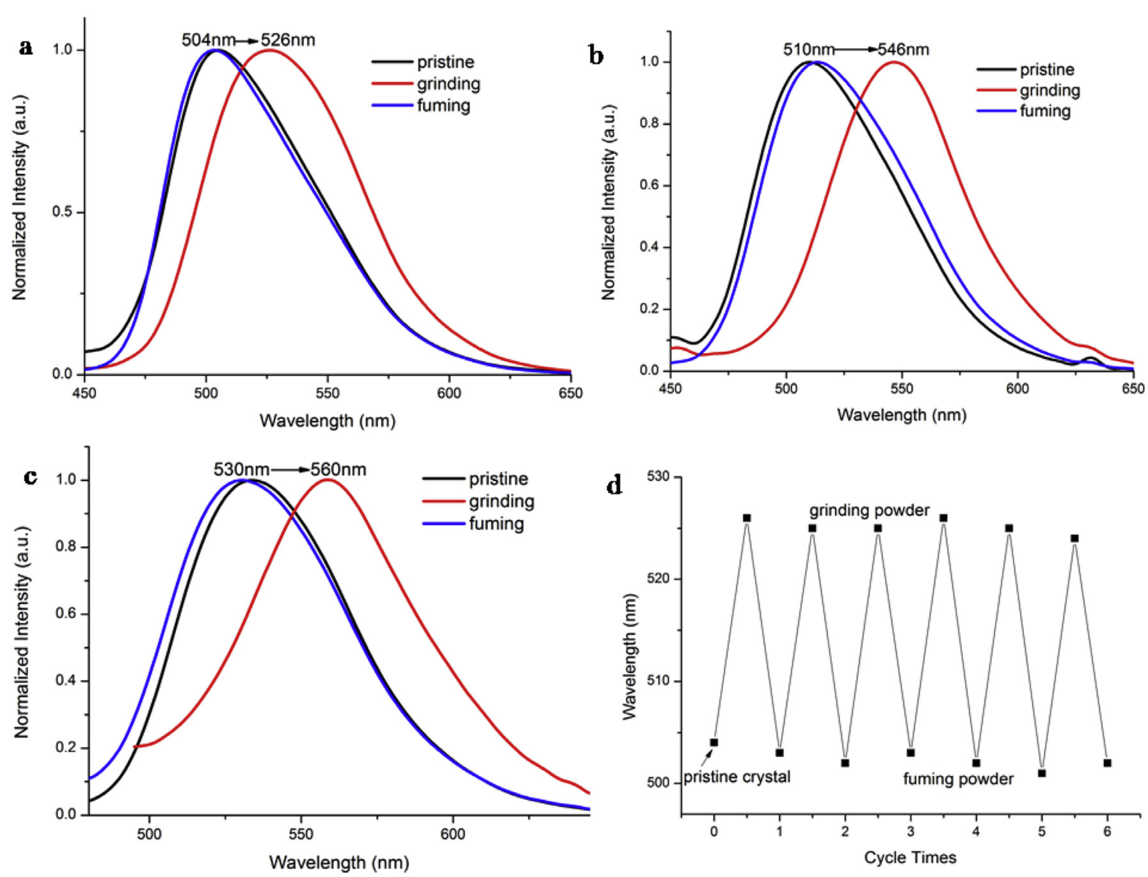

Fig. 7. Normalized fluorescence spectra of **T1** (a), **T2** (b), and **T3** (c) in different solid states: pristine, grinding and fuming (excited at 380 nm for **T1**, 420 nm for **T2**, 435 nm for **T3**); (d) Maximum fluorescence emission of **T1** upon treated by grinding and fuming with DCM repeatedly.

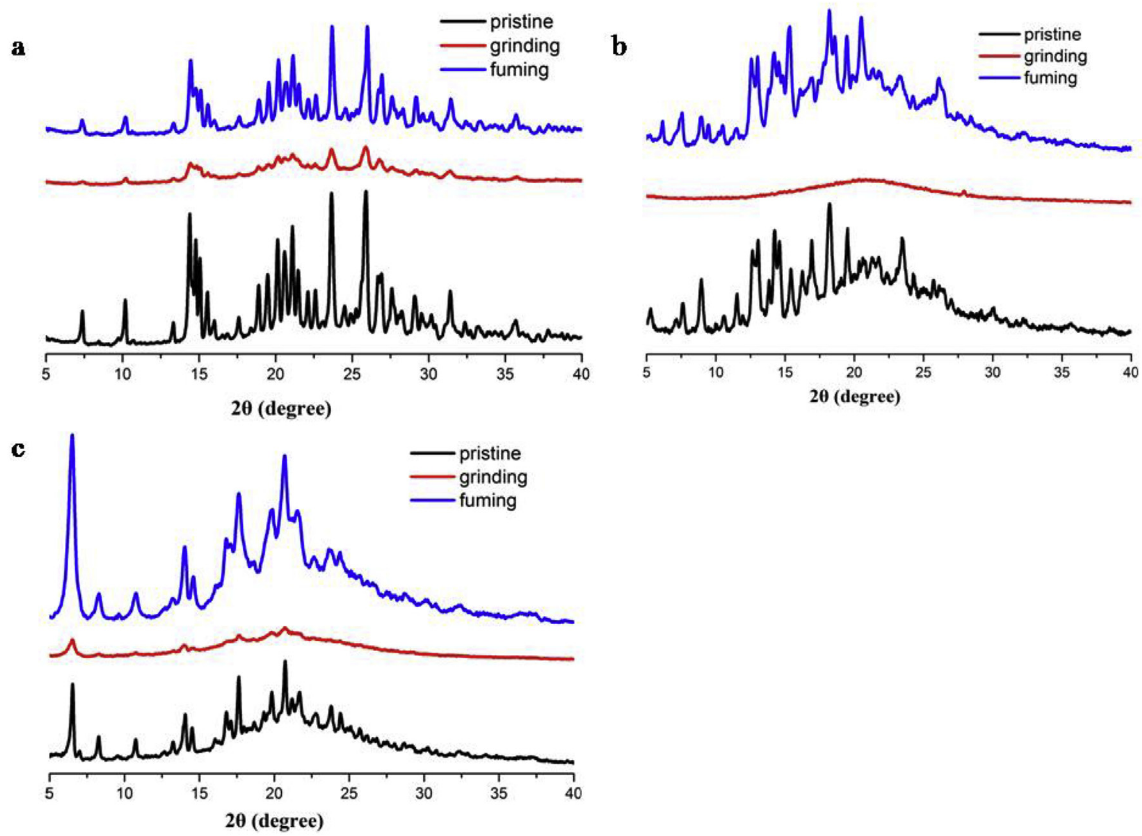

Fig. 8. PXRD patterns of (a) **T1**, (b) **T2**, and (c) **T3** in different solid states: pristine, grinding and fuming.

normalized fluorescence emission spectra of samples in different solid states (pristine, grinding and fuming) are shown in Fig. 7. It was clear that the emission peaks of **T1**, **T2** and **T3** in the pristine crystals appeared at 504, 510 and 530 nm and red-shifted to 526, 546 and 560 nm in the ground powders, respectively, indicating that the grinding treatment induced the spectral bathochromic shifts of 22, 36 and 30 nm for **T1**, **T2** and **T3** (Table S4, ESI). In addition, after fuming with DCM for several seconds, the emission colors were restored to the original states, similar to their pristine crystals, and the corresponding maximum fluorescence wavelengths could blue-shift to the pristine crystals. If the fuming powders were reground, their emission colors were again changed as the first grinding. This MFC conversion could be repeated many times without fatigue (Fig. 7d and Fig. S4, ESI), indicating excellent reversibility in the switching processes. In contrast, when the ground powders of the three compounds were heated at certain temperature, the emissions could not be converted back to their original states. Compared with **T1**, **T2** and **T3** with electron-donating groups exhibited the larger spectral shifts ($\Delta\lambda$ = 36 nm for **T2** and $\Delta\lambda$ = 30 nm for **T3**) after grinding the pristine crystal (Table S4, ESI), which could be ascribable to the key role of the ICT transition, which was well-known to contribute greatly to MFC behavior with higher sensitivity toward mechanical force [23]. Besides, **T2** exhibited a high-contrast MFC relative to **T3**. The reason might be that the *tert*-butyl group could made the molecule more twisted and loosely packed through its steric hindrance effect [24].

To understand the mechanism of the MFC behaviors of **T1**, **T2** and **T3**, the powder wide-angle X-ray diffraction (PXRD) measurements were conducted. According to the PXRD measurements, **T1**, **T2** and **T3** formed different molecular aggregates before and after grinding treatment. As shown in Fig. 8, it was clear that the PXRD patterns of the pristine crystals exhibited many strong and sharp diffraction peaks, indicating a well-ordered microcrystalline-like structures. After grinding, the PXRD patterns displayed significant decreased peak intensity but increased peak widths, indicating that the crystalline phase was damaged into amorphous state during the grinding process, which resulted in the different fluorescence emission spectra of the ground powders [25]. However, when the ground powders were treated by DCM fuming, sharp and intense diffraction peaks could be appeared into an ordered crystalline phase. Therefore, the mechanochromism of the three compounds was attributed to the transformations between the ordered crystalline and amorphous states.

Differential scanning calorimetry (DSC) measurements were performed to further study their thermal properties. The DSC curves of **T1**, **T2** and **T3** in different solid states are shown in Fig. 9. It was found that the DSC curves of the pristine crystals of **T1**, **T2** and **T3** exhibited only a single endothermal peak at 228 °C, 170 °C and 205 °C, respectively, corresponding to their melting points. However, the ground powders of **T1** and **T3** showed an additional one exothermic peak at 113 °C and 95 °C, respectively, and the ground powder of **T2** exhibited two weak exothermic transition peaks at 106 °C and 147 °C before melting point, which could be assigned to their cold-crystallization temperature, and also demonstrated that the amorphous state was a metastable state [26]. **T1**, **T2** and **T3** possessed an additional metastable state, which could be converted to a crystalline state upon thermal annealing, indicating the phase transition form a poorly organized phase to a well-ordered phase.

When a filter paper containing the pristine solids of **T1**, **T2** and **T3** were pressed by streaking a stainless steel pen, a color trails were observed. As shown in Fig. 10a, three English letters, "BZY", with yellowish green fluorescence under UV irradiation were written using a ball pen. The three letters were hidden by DCM vapor fuming for 10 s, and the entire solid film emitted green fluorescence under 365 nm light. Similarly, **T2** and **T3** solid film might be used as recording material (Fig. 10b and c). Bright yellow letters "BZY" could be written in green (**T2** solid) and yellowish green (**T3** solid) background, and could be erased after fuming DCM vapor. Thus, these solid film based on BOPIM

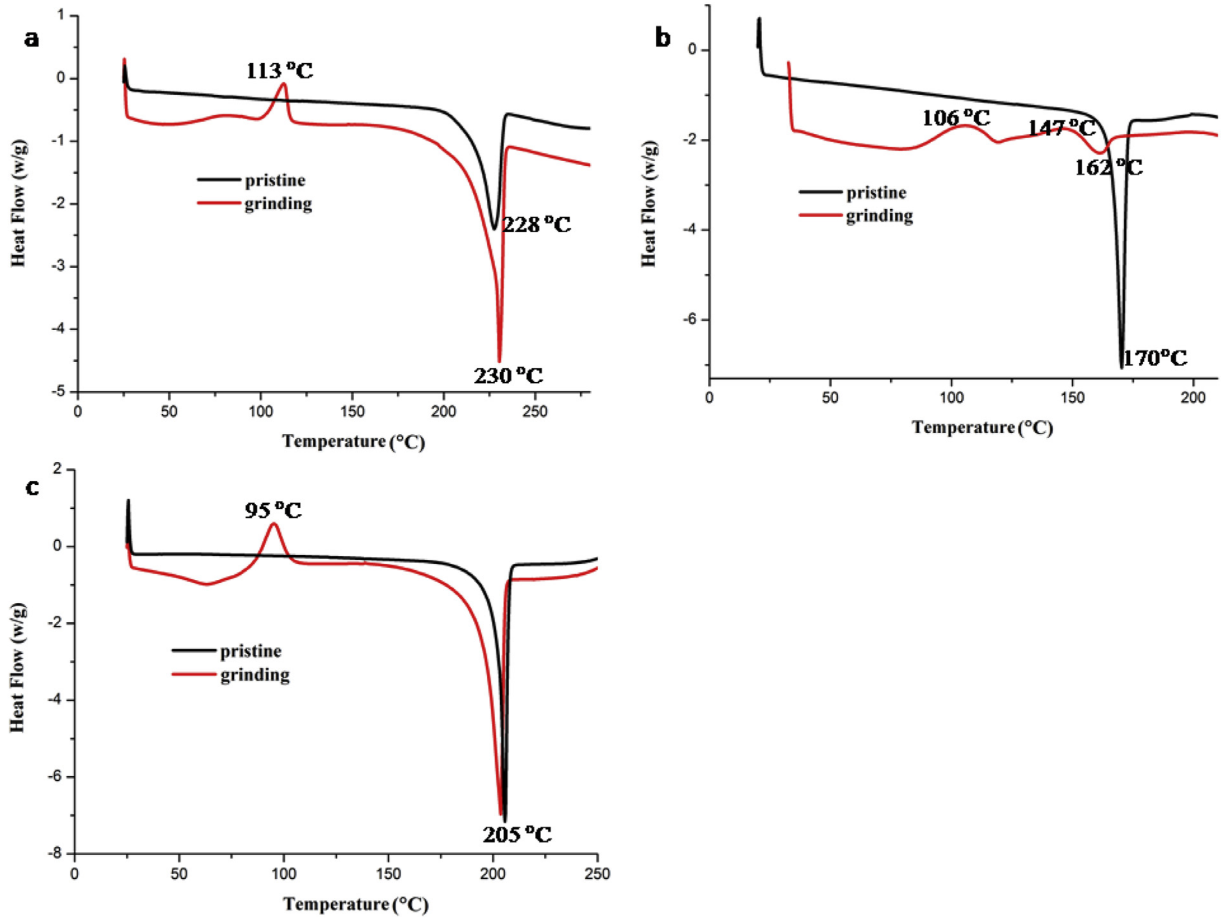

Fig. 9. DSC curves of compounds **T1** (a), **T2** (b) and **T3** (c) for the pristine crystals and ground powders under nitrogen atmosphere at a heating rate of 10 °C/min.

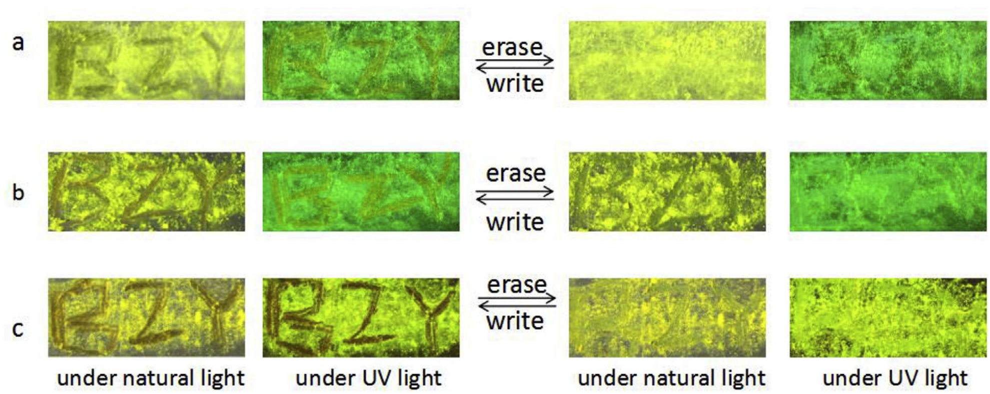

Fig. 10. Photographic images of (a) **T1**, (b) **T2**, and (c) **T3** films on pieces of filter paper in response to grinding, fuming under the irradiation of 365 nm UV light.

dyes as a smart materials can be used to record information.

4. Conclusions

In summary, a series of BOPIM complexes was obtained by introducing different substituents (including bromo, *tert*-butyl and methoxyl) on the benzene ring of BOPIM dyes. Their molecular structure, photophysical properties and MFC behaviors have been investigated and compared. Single crystal structure illustrated that the non-planar orientation of BOPIM dyes. Spectral measurements and quantum chemical calculation indicated a push-pull electronic structure and non-planar geometry, and they gave unique ICT emission in dilute solutions. Reversible mechanofluorochromism were detected for the three synthesized complexes. The solid emission studies of **T1**, **T2** and **T3** illustrated that their emission color could change reversibly upon the treatment of grinding and fuming with DCM. The MFC behaviors of these three compounds increased with the same order of **T1** < **T3** < **T2**, which depended on electronic and steric effects of the peripheral substituents on the BOPIM dyes. Moreover, information written by force can be hidden using DCM vapor. Thus, BOPIM dyes could act as smart materials for data security protection. The current studies provided valuable information for designing new MFC materials that have potential application in optical-recording materials.

Acknowledgements

This work was financially supported by foundation of scientific research start-up of China Jiliang University (No. 000617).

Appendix A. Supplementary data

Supplementary data to this article can be found online at https://doi.org/10.1016/j.dyepig.2019.04.001.

References

[1] (a) Das S, Heasman P, Ben T, Qiu S. Porous organic materials: strategic design and structure-function correlation. Chem Rev 2017;117:1515–63;
(b) Mei J, Leung NLC, Kwok RTK, Lam JWY, Tang BZ. Aggregation-induced emission: together we shine, united we soar. Chem Rev 2015;115:11718–940;
(c) Pu L. Simultaneous determination of concentration and enantiomeric composition in fluorescent sensing. Acc Chem Res 2017;50:1032–40.

[2] (a) Chi Z, Zhang X, Xu B, Zhou X, Ma C, Zhang Y, Liu S, Xu J. Recent advances in organic mechanofluorochromic materials. Chem Soc Rev 2012;41:3878–96;
(b) Xue P, Ding J, Wang P, Lu R. Recent progress in the mechanochromism of phosphorescent organic molecules and metal complexes. J Mater Chem C 2016;4:6688–706;
(c) Wang C, Li Z. Molecular conformation and packing: their critical roles in the emission performance of mechanochromic fluorescence materials. Mater Chem Front 2017;1:2174–94.

[3] (a) Biswas S, Jana D, Kumar S, Maji S, Kundu P, Ghorai UK, et al. Supramolecular aggregates of tetraphenylethene-cored AIEgen toward mechanoluminescent and electroluminescent devices. ACS Appl Mater Interfaces 2018;10:17409–18;
(b) Xiong J, Wang K, Yao Z, Zou B, Xu J, Bu X-H. Multi-stimuli-responsive fluorescence switching from a pyridine-functionalized tetraphenylethene AIEgen. ACS Appl Mater Interfaces 2018;10:5819–27;
(c) Huang L, Qiu Y, Wu C, Ma Z, Shen Z, Jia X. A multi-state fluorescent switch with multifunction of AIE, methanol-responsiveness, photochromism and mechanochromism. J Mater Chem C 2018;6:10250–5.

[4] (a) Pei S, Chen X, Zhou Z, Zou H, Gong Y. Dyes Pigm 2018;154:113–20;
(b) Gong Y, Zhang Y, Yuan WZ, Sun JZ, Zhang Y. D-A solid emitter with crowded and remarkably twisted conformations exhibiting multifunctionality and multicolor mechanochromism. J Phys Chem C 2014;118:10998–1005.

[5] (a) Feng H-T, Yuan Y-X, Xiong J-B, Zheng Y-S, Tang BZ. Macrocycles and cages based on tetraphenylethylene with aggregation-induced emission effect. Chem Soc Rev 2018;47:7452–76;
(b) Zhao J, Chi Z, Zhang Y, Mao Z, Yang Z, Ubba E, Chi Z. Recent progress in the mechanofluorochromism of cyanoethylene derivatives with aggregation-induced emission. J Mater Chem C 2018;6:6327–53.

[6] (a) Xiong Y, Yan X, Ma Y, Li Y, Chen L. Regulating the piezofluorochromism of 9,10-bis(butoxystyryl)anthracenes by isomerization of butyl groups. Chem Commun 2015;51:3403–6;
(b) Zheng M, Zhang D, Sun M, Li Y, Liu T, Xue S, Yang WJ. Cruciform 9,10-distyryl-2,6-bis(*p*-dialkylamino-styryl)anthracene homologues exhibiting alkyl length-tunable piezochromic luminescent and heat-recovery temperature of ground states. J Mater Chem C 2014;2:1913–20.

[7] (a) Yoshii R, Suenaga K, Tanaka K, Chujo Y. Mechanofluorochromic materials based on aggregation-induced emission-active boron ketoiminates: regulation of the direction of the emission color changes. Chem Eur J 2015;21:7231–7;
(b) Yoshii R, Hirose A, Tanaka K, Chujo Y. Boron diiminate with aggregation-induced emission and crystallization-induced emission-enhancement characteristics. Chem Eur J 2014;20:8320–4.

[8] (a) Suzuki T, Okada H, Nakagawa T, Komatsy K, et al. A fluorenylidene-acridane that becomes dark in color upon grinding-ground state mechanochromism by conformational change. Chem Sci 2018;9:475–82;
(b) Hariharan PS, Mothi EM, Moon D, Anthony SP. Halochromic isoquinoline with mechanochromic triphenylamine: smart fluorescent material for rewritable and self-erasable fluorescent platform. ACS Appl Mater Interfaces 2016;8:33034–42.

[9] Ma C, Zhang X, Yang Y, Ma Z, Yang L, Wu Y, Liu H, Jia X, Wei Y. Effect of alkyl length dependent crystallinity for the machanofluorochromic feature of alkyl phenothiazinyl tetraphenylethenyl acrylonitrile derivatives. J Mater Chem C 2016;4:4786–91.

[10] (a) Guo C, Li M, Yuan W, Wang K, Zou B, Chen Y. Tuning the mechanochromic luminescence of BOPIM complexes by rational introduction of aromatic substituents. J Phys Chem C 2017;121:27009–17;
(b) Jadhav T, Dhokale B, Misra R. Effect of the cyano group on solid state photophysical behavior of tetraphenylethene substituted benzothiazoles. J Mater Chem C 2015;3:9063–8;
(c) Jadhav T, Choi JM, Dhokale B, Mobin SM, Lee JY, Misra R. Effect of end groups on mechanochromism and electroluminescence in tetraphenylethylene substituted phenanthroimidazoles. J Phys Chem C 2016;120:18487–95.

[11] (a) Ibarra-Rodríguez M, Muñoz-Flores BM, Rasika Dias HV, Sánchez M, et al. J Org Chem 2017;82:2375–85;
(b) Lugovik KI, Eltyshev AK, Suntsova PO, Slepukhin PA, et al. Highlights on the road towards highly emitting solid-state luminophores: two classes of thiazole-based organoboron fluorophores with the AIEE/AIE effect. Chem Asian J 2018;13:311–24.

[12] Dhokale B, Jadhav T, Mobin SM, Misra R. Meso alkynylated tetraphenylethylene (TPE) and 2,3,3-triphenylacrylonitrile (TPAN) substituted BODIPYs. J Org Chem 2015;80:8018–25.

[13] Wang S, Tan R, Li Y, Li Q, Xiao S. Solid state emission and mechanochromic luminescence of boron 2-(2-'-pyridyl)imidazole complexes. Dyes Pigm 2016;132:342–6.

[14] Wang S, Xiao S, Chen X, Zhang R, Cao Q, Zou K. Crystalline solid responsive to mechanical and acidic stimuli:boron-fluorine derivative with TICT characteristic. Dyes Pigm 2013;99:543–7.

[15] (a) Yang W, Liu C, Lu S, Du J, Gao Q, Zhang R, Liu Y, Yang C. AIE-active smart cyanostyrene luminogens: polymorphism-dependent multicolor mechanochromism. J Mater Chem C 2018;6:290–8;
(b) Ramachandran E, Dhamodharan R. Tetrakis(trialkylsilylethynylphenyl) ethenes: mechanofluorochromism arising from steric considerations with an unusual crystal structure. J Mater Chem C 2017;5:10469–76.

[16] Li W, Lin W, Wang J, Guan X. Phenanthro[9,10-d]imidazole-quinoline boron difluoride dyes with solid-state red fluorescence. Org Lett 2013;15:1768–71.

[17] Li Z, Lv X, Chen Y, Fu W-F. Synthesis, structures and photophysical properties of boron-fluorine derivatives based on pyridine/1,8-naphthyridine. Dyes Pigm 2014;105:157–62.

[18] (a) Zhan Y, Xu Y, Jin Z, Ye W, Yang P. Phenothiazine substituted phenanthroimidazole derivatives: synthesis, photophysical properties and efficient piezochromic luminescence. Dyes Pigm 2017;140:452–9;
(b) Zhang G, Sun J, Xue P, Zhang Z, Gong P, Peng J, Lu R. Phenothiazine modified triphenylacrylonitrile derivates: AIE and mechanochromism tuned by molecular conformation. J Mater Chem C 2015;3:2925–32.

[19] (a) Zhan Y, Yang P, Li G, Bao Y. Reversible piezofluorochromism of a triphenylamine-based benzothiazole derivative with a strong fluorescence response to volatile acid vapors. New J Chem 2017;41:263–70;
(b) Gao H, Xu D, Wang Y, Zhang C, et al. Aggregation-induced emission and mechanofluorochromism of tetraphenylbutadiene modified β-ketoiminate boron complexes. Dyes Pigm 2018;150:165–73.

[20] Zhao H, Wang Y, Harrington S, Ma L, Hu S, et al. Remarkable substitution influence on the mechanochromism of cyanostilbene derivatives. RSC Adv 2016;6:66477–83.

[21] Wang Y, Xu D, Gao H, Wang Y, et al. Mechanofluorochromic properties of aggregation-induced emission-active tetraphenylethene-containing cruciform luminophores. Dyes Pigm 2018;156:291–8.

[22] Lu Q, Li X, Li J, Yang Z, Xu B, Chi Z, Xu J, Zhang Y. Influence of cyano groups on the properties of piezofluorochromic aggregation-induced emission enhancement compounds derived from tetraphenylvinyl-capped ethane. J Mater Chem C 2015;3:1225–34.

[23] (a) Zhang Y, Wang K, Zhuang G, Xie Z, Zhang C, et al. Multicolored-fluorescence switching of ICT-type organic solids with clear color difference: mechanically controlled excited state. Chem Eur J 2015;21:2474–9;
(b) Zhan Y, Gong P, Yang P, Jin Z, Bao Y, Li Y, Xu Y. Aggregation-induced emission and reversible mechanochromic luminescence of carbazole-based triphenylacrylonitrile derivatives. RSC Adv 2016;6:32697–704.

[24] Gong P, Yang H, Sun J, Zhang Z, Sun J, Xue P. Salicylaldimine difluoroboron complexes containing tert-butyl groups: nontraditional π-gelator and piezofluorochromic compounds. J Mater Chem C 2015;3:10302–8.

[25] (a) Roy B, Reddy MC, Hazra P. Developing the structure-property relationship to design solid state multi-stimuli responsive materials and their potential applications in different fields. Chem Sci 2018;9:3592–606;
(b) Chen Y, Ling Y, Xiang C, Zhou G. Quinoxalie-based cross-conjugated luminophores: charge transfer, piezofluorochromic, and sensing properties. J Mater Chem C 2016;4:8496–505.

[26] Jiang Y, Gindre D, Allain M, Liu P, Cabanetos C, Roncali J. A mechanofluorochromic push-pull small molecule with aggregation-controlled linear and nonlinear optical properties. Adv Mater 2015;27:4285–9.